SR-70

November 1962

DYNAMIC STRESSES AND DISPLACEMENTS AROUND CYLINDRICAL DISCONTINUITIES DUE TO PLANE SHEAR WAVES

C.C. Mow

L.J. Mente

THE MITRE CORPORATION

SR-70

DYNAMIC STRESSES AND DISPLACEMENTS AROUND CYLINDRICAL DISCONTINUITIES DUE TO PLANE SHEAR WAVES

by

C.C. Mow

L.J. Mente

November 1962

THE MITRE CORPORATION

Box 208

Bedford, Massachusetts

Contract AF-33(600)39852
Project 607

ABSTRACT

The problem of dynamic stresses and displacements around a cavity and rigid inclusion of arbitrary density is examined for an elastic medium during the passage of a plane shear wave. In the cavity case, the dynamic stresses and displacements are found to be dependent upon the incident wave number and Poisson's ratio of the medium. In the rigid inclusion case, it is found that dynamic stresses and the rigid body rotation and translation are dependent upon the incident wave numbers, the Poisson's ratio, and the density ratio of the medium and the insert. Close coupling is observed between the stresses and the rigid body motion of the insert.

ACKNOWLEDGMENT

The authors wish to thank Mr. C. McCarthy of Department D-19 of The MITRE Corporation for his able assistance in obtaining the numerical results.

CONTENTS

INTRODUCTION

The problem of dynamic stress concentration, around a cylindrical discontinuity in an infinite elastic medium, subjected to a plane travelling wave has been under extensive study in recent years. [1, 2, 3, 4, 5] Former investigations, however, considered only the case where the incident wave is a plane compressional wave. In this paper, the dynamic stresses due to an incident, plane, shear wave are investigated. Two cylindrical discontinuities are considered: a cavity, and a rigid inclusion of arbitrary density. Furthermore, the displacements on the cavity's free surface and the rigid body translation and rotation of the rigid inclusion are also determined.

In the approach presented here, the incident shear wave is assumed to vary harmonically with time. At the boundary of the discontinuity, incident waves will be reflected into compressional and shear waves. The resultant dynamic stresses around the cylindrical discontinuity can be found from the solutions of the scattered waves and the incident waves near the obstacle. The solutions obtained are based on the generalized plane strain assumption.

Comparisons are made between Kirsch's [6] static solution for the cavity case and Goodier's [7] static solution for the rigid inclusion with the present solution. As the wave numbers become small, the dynamic cavity solution reduces to the static solution. The dynamic solution for

the rigid inclusion also reduces to the static solution for any finite inclusion density. However, when the inclusion density is infinite (which is the same as holding the inclusion fixed in space) a singularity will occur as the wave numbers approach zero. A similar phenomenon was discussed in detail by Pao and Mow. [4]

GENERAL THEORY

Under the generalized plane strain assumption, the displacement equations of motion are

$$(\lambda + \mu)\nabla\,\nabla \cdot \underset{\sim}{u} + \mu\,\nabla^2\,\underset{\sim}{u} = \rho\,\ddot{\underset{\sim}{u}} \tag{1}$$

where

$\underset{\sim}{u}$ is the displacement vector

∇ is the vector differential operator

λ and μ are the Lamé constants

ρ is the density

The displacement vector $\underset{\sim}{u}$, under the Helmholtz theorm, can be represented in terms of a scalar potential and a vector potential. In the case of plane strain, this displacement vector is given by

$$\underset{\sim}{u} = \nabla\,\varphi + \nabla \times (\underset{\sim}{e}_z\,\psi) \tag{2}$$

where $\underset{\sim}{e}_z$ is a unit vector along the axis of the cylindrical discontinuity. Each potential function then satisfies a scalar wave equation

$$c_\alpha^2 \nabla^2 \varphi = \ddot{\varphi} \tag{3}$$

$$c_\beta^2 \nabla^2 \psi = \ddot{\psi} \tag{4}$$

where

$$c_\alpha^2 = \frac{\lambda + 2\mu}{\rho}$$

$$c_\beta^2 = \frac{\mu}{\rho}$$

INCIDENT AND REFLECTED WAVES

An incident plane shear wave propagating in the positive x direction is represented by

$$\begin{aligned} \psi^{(i)} &= \psi_0 e^{i(\beta x - \omega t)} \\ \varphi^{(i)} &= 0 \end{aligned} \tag{5}$$

where

ψ_0 is the measure of amplitude

ω is the circular frequency

$\beta = \omega/c_\beta$ is the wave number of the shear wave

Equation (5) can be expressed in polar coordinates

$$\psi^{(i)} = \psi_0 \sum_{n=0}^{\infty} \epsilon_n i^n J_n(\beta r) \cos n\theta e^{-i\omega t} \tag{6}$$

where

$$\epsilon_n = \begin{cases} 1 & n=0 \\ 2 & n \geq 1 \end{cases}$$

If the origin of the polar coordinates is selected at the center of the cylindrical discontinuity (Fig. 1), the reflected waves can be expressed as

$$\varphi^{(r)} = \sum_{n=0}^{\infty} A_n H_n(\alpha r) \sin n\theta e^{-i\omega t} \tag{7}$$

$$\psi^{(r)} = \sum_{n=0}^{\infty} B_n H_n(\beta r) \cos n\theta e^{-i\omega t} \tag{8}$$

where

A_n and B_n are expansion coefficients to be determined by the appropriate boundary conditions

$\alpha = \omega/c_\alpha$ is the compressional wave number

H_n denotes the Hankel function of the first kind of order n.

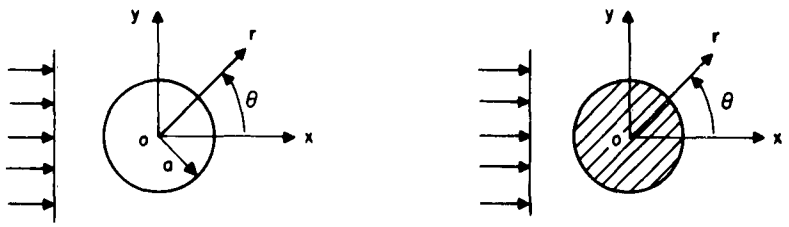

CYLINDRICAL CAVITY RIGID CYLINDRICAL INCLUSION

Fig. 1

The total potential can then be determined by superimposing the incident and reflected potentials. Thus, the displacement potentials are

$$\varphi = \varphi^{(i)} + \varphi^{(r)} = \varphi^{(r)}$$

$$\psi = \psi^{(i)} + \psi^{(r)} \qquad (9)$$

Substitution of Equations (6) - (9) into the well-known relationships [4] between stresses, displacements and displacement potentials yields the corresponding stress and displacement components. With the time factor $e^{-i\omega t}$ omitted, they are given by

$$\tau_{rr} = 2\mu r^{-2} \sum_{n=0}^{\infty} (\psi_0 \epsilon_n i^n {}_0D_{1n} + A_n {}_1D_{1n} + B_n {}_2D_{1n}) \sin n\theta$$

$$\tau_{\theta\theta} = 2\mu r^{-2} \sum_{n=0}^{\infty} (\psi_0 \epsilon_n i^n {}_0D_{2n} + A_n {}_1D_{2n} + B_n {}_2D_{2n}) \sin n\theta \qquad (10)$$

$$\tau_{r\theta} = 2\mu r^{-2} \sum_{n=0}^{\infty} (\psi_0 \epsilon_n i^n {}_0D_{3n} + A_n {}_1D_{3n} + B_n {}_2D_{3n}) \cos n\theta$$

and

$$u_r = -r^{-1} \sum_{n=0}^{\infty} (\psi_0 \epsilon_n i^n {}_0D_{4n} - A_n {}_1D_{4n} + B_n {}_2D_{4n}) \sin n\theta$$

$$u_\theta = -r^{-1} \sum_{n=0}^{\infty} (\psi_0 \epsilon_n i^n {}_0D_{5n} - A_n {}_1D_{5n} + B_n {}_2D_{5n}) \cos n\theta \qquad (11)$$

In Equations (10) and (11), ${}_0D_{1n}$ through ${}_0D_{5n}$ represents the contribution on stresses and displacements by the incident wave, while ${}_1D_{1n} - {}_1D_{5n}$ and ${}_2D_{1n} - {}_2D_{5n}$ represents the contribution on stresses and displacements by the reflected compressional and shear waves, respectively. These functions are defined

$$
\begin{aligned}
{}_0D_{1n} &= n(n+1)\, J_n(\beta r) - n\beta r\, J_{n-1}(\beta r) \\
{}_0D_{2n} &= -n(n+1)\, J_n(\beta r) + n\beta r\, J_{n-1}(\beta r) \\
{}_0D_{3n} &= -\left(n^2+n-\frac{\beta^2 r^2}{2}\right) J_n(\beta r) + \beta r\, J_{n-1}(\beta r) \\
{}_0D_{4n} &= n J_n(\beta r) \\
{}_0D_{5n} &= -n J_n(\beta r) + \beta r\, J_{n-1}(\beta r)
\end{aligned}
\tag{12}
$$

$$
\begin{aligned}
{}_1D_{1n} &= \left(n^2+n-\frac{\beta^2 r^2}{2}\right) H_n(\alpha r) - \alpha r\, H_{n-1}(\alpha r) \\
{}_1D_{2n} &= -\left(n^2+n-\alpha^2 r^2+\frac{\beta^2 r^2}{2}\right) H_n(\alpha r) + \alpha r\, H_{n-1}(\alpha r) \\
{}_1D_{3n} &= -(n^2+n)\, H_n(\alpha r) + n\alpha r\, H_{n-1}(\alpha r) \\
{}_1D_{4n} &= -n\, H_n(\alpha r) + \alpha r\, H_{n-1}(\alpha r) \\
{}_1D_{5n} &= n\, H_n(\alpha r)
\end{aligned}
\tag{13}
$$

$$
\begin{aligned}
{}_2D_{1n} &= n(n+1)\, H_n(\beta r) - n\beta r\, H_{n-1}(\beta r) \\
{}_2D_{2n} &= -n(n+1)\, H_n(\beta r) + n\beta r\, H_{n-1}(\beta r) \\
{}_2D_{3n} &= -\left(n^2+n-\frac{\beta^2 r^2}{2}\right) H_n(\beta r) + \beta r\, H_{n-1}(\beta r) \\
{}_2D_{4n} &= n H_n(\beta r) \\
{}_2D_{5n} &= -n H_n(\beta r) + \beta r\, H_{n-1}(\beta r)
\end{aligned}
\tag{14}
$$

BOUNDARY CONDITIONS AND SOLUTIONS

As previously mentioned, the coefficients A_n and B_n are to be determined by the appropriate boundary conditions associated with the two types of discontinuities considered: the cavity and the rigid inclusion. The appropriate boundary condition for the cavity case is obvious; i.e., traction free at the boundary. The boundary condition for the rigid inclusion, however, is not this clear.[4] The correct boundary condition in this case is obtained by leaving the rigid inclusion free to rotate as well as translate with the surrounding medium. This implies that, at the interface, the displacements due to the combined incident and reflected waves are equal to the displacements corresponding to the rigid body rotation and translation of the inclusion which are determined by the application of Newton's law of motion.

Cavity

The boundary conditions at $r = a$, where a is the radius of the cylindrical discontinuity, are given by

$$\tau_{rr} = \tau_{r\theta} = 0$$

If each term of the series for τ_{rr} and $\tau_{r\theta}$ in Equation (10) is set equal to zero at $r = a$, the coefficients A_n and B_n are determined from a pair of equations for each value of n

$$A_n = -\frac{\psi_0 \epsilon_n i^n}{\Delta_n} \begin{vmatrix} {}_0\bar{D}_{1n} & {}_2\bar{D}_{1n} \\ {}_0\bar{D}_{3n} & {}_2\bar{D}_{3n} \end{vmatrix} \tag{15}$$

$$B_n = -\frac{\psi_0 \epsilon_n i^n}{\Delta_n} \begin{vmatrix} {}_1\bar{D}_{1n} & {}_0\bar{D}_{1n} \\ {}_1\bar{D}_{3n} & {}_0\bar{D}_{3n} \end{vmatrix} \tag{16}$$

and

$$\Delta_n = \begin{vmatrix} {}_1\bar{D}_{1n} & {}_2\bar{D}_{1n} \\ {}_1\bar{D}_{3n} & {}_2\bar{D}_{3n} \end{vmatrix} \tag{17}$$

where ${}_0\bar{D}_{1n} \cdots {}_2\bar{D}_{3n}$ denote the value of ${}_0D_{1n} \cdots {}_2D_{3n}$ at r = a. The displacements and stress can then be calculated by the substitution of Equations (15) through (17) into Equations (10) and (11), and the solution is complete.

It is convenient to nondimensionalize the stresses and displacements with respect to the dimensional coefficient of the stress and displacement associated with the incident wave, i.e., $\tau_0 = \mu\beta^2\psi_0$ and $u_0 = -i\beta\psi_0$. It is noted that the wave number is normalized by the radius of the circular inclusion. Thus, the dimensionless wave numbers αa and βa may be regarded as the ratio of the circumference to the incident wave length. Thus, at the boundary (r = a) the dimensionless stress $\tau^*_{\theta\theta}$ and displacements u^*_r and u^*_θ are given in the following form

$$\tau^*_{\theta\theta} = -\frac{8}{\pi}\left(1 - \frac{1}{k^2}\right) \sum_{n=1}^{\infty} i^{n+1} \frac{n\left(n^2 - 1 - \frac{\beta^2 a^2}{2}\right) H_n(\alpha a)}{\Delta_n} \sin n\theta \tag{18}$$

$$u^*_r = -\frac{2\beta a}{\pi} \sum_{n=1}^{\infty} \frac{n i^n \left[(n+1)H_n(\alpha a) - \alpha a\, H_{n-1}(\alpha a)\right]}{\Delta_n} \sin n\theta \tag{19}$$

$$u_\varphi^* = -\frac{\beta a}{\pi} \sum_{n=0}^{\infty} \frac{\epsilon_n i^n \left[\left(n^2+n-\frac{\beta^2 a^2}{2}\right) H_n(\alpha a) - \alpha a H_{n-1}(\alpha a) \right]}{\Delta_n} \cos n\theta \tag{20}$$

where

$$k^2 = \frac{\beta^2}{\alpha^2} = \frac{c_\alpha^2}{c_\beta^2} = \frac{2(1-\sigma)}{(1-2\sigma)}$$

σ is the Poisson's ratio.

Rigid Inclusion of Arbitrary Density

As previously discussed, the rigid inclusion in general will rotate and translate with the surrounding medium. The resultant forces and torque acting on the inclusion as a result of the stresses acting on the boundary due to the incident and reflected waves are expressed by

$$F_x = \int_0^{2\pi} (\bar{\tau}_{rr} \cos\theta - \bar{\tau}_{r\theta} \sin\theta)\, a\, d\theta \tag{21}$$

$$F_y = \int_0^{2\pi} (\bar{\tau}_{rr} \sin\theta + \bar{\tau}_{r\theta} \cos\theta)\, a\, d\theta \tag{22}$$

$$T = \int_0^{2\pi} \bar{\tau}_{r\theta}\, a^2 d\theta \tag{23}$$

By substituting Equation (10) with $r = a$ into Equations (21) through (23) and considering the orthogonality, it can be readily shown that

$$F_x = 0 \tag{24}$$

$$F_y = 2\mu a^{-1} \pi [2\psi_0 \, i \, ({}_0\bar{D}_{11} + {}_0\bar{D}_{31}) + A_1 \, ({}_1\bar{D}_{11} + {}_1\bar{D}_{31}) + B_1 \, ({}_2\bar{D}_{11} + {}_2\bar{D}_{31})] \tag{25}$$

and

$$T = 4\pi\mu \, [\psi_0 \, {}_0\bar{D}_{30} + A_0 \, {}_1\bar{D}_{30} + B_0 \, {}_2\bar{D}_{30}] \tag{26}$$

From Newton's law of motion, it is known that

$$(\pi a^2 \rho_1) \, \ddot{U}_y = F_y \tag{27}$$

$$\left(\frac{\pi \rho_1 a^4}{2} \right) \ddot{\Theta} = T \tag{28}$$

By restoring the time factor $e^{-i\omega t}$, which is omitted in Equation (10), and twice integrating Equations (27) and (28) with respect to time, the rigid body translation and rotation of the inclusion is found to be given by

$$U_y = \frac{2\eta}{\beta^2 a^3} \left[2\psi_0 i \left({}_0\bar{D}_{11} + {}_0\bar{D}_{31} \right) + A_1 \left({}_1\bar{D}_{11} + {}_1\bar{D}_{31} \right) + B_1 \left({}_2\bar{D}_{11} + {}_2\bar{D}_{31} \right) \right] \tag{29}$$

$$\Theta = -\frac{8\eta}{\beta^2 a^4} \left(\psi_0 \, {}_0\bar{D}_{30} + A_0 \, {}_1\bar{D}_{30} + B_0 \, {}_2\bar{D}_{30} \right) \tag{30}$$

where $\eta = \frac{\rho_0}{\rho_1}$ is the ratio of density of the surrounding medium to that of the inclusion. The translation and the rotation will vanish if $\eta = 0$. Hence, the problem is the same as the case when the inclusion is fixed in space.

For any inclusion with finite density, the displacements at the boundary of the inclusion must be

$$\bar{u}_r = U_y \sin\theta$$

$$\bar{u}_\theta = U_y \cos\theta + a\Theta \tag{31}$$

If the expressions for $\bar{u}_r$ and $\bar{u}_\theta$ in Equation (11) are substituted into Equation (31) and the orthogonality conditions are employed, it is found that for

$n = 0$

$$A_0 = 0$$

$$B_0 = -\psi_0 \frac{\beta^2 a^2 J_1(\beta a) + 8\eta \left[\frac{\beta a}{2} J_0(\beta a) - J_1(\beta a) \right]}{\beta^2 a^2 H_1(\beta a) + 8\eta \left[\frac{\beta a}{2} H_0(\beta a) - H_1(\beta a) \right]} \tag{32}$$

$n = 1$

$$A_1 = -\frac{2i\psi_0}{\delta_1} \beta a(1-\eta) \left[J_1(\beta a) H_0(\beta a) - J_0(\beta a) H_1(\beta a) \right]$$

$$B_1 = -\frac{2i\psi_0}{\delta_1} \left[-4\eta J_1(\beta a) H_1(\alpha a) + (1+\eta) \left(\beta a H_1(\alpha a) J_0(\beta a) + \alpha a J_1(\beta a) H_0(\alpha a) \right) - \alpha\beta a^2 J_0(\beta a) H_0(\alpha a) \right] \tag{33}$$

$n \geq 2$

$$A_n = -\frac{2\psi_0 n i^n \beta a}{\Delta_n} \left[J_n(\beta a) H_{n-1}(\beta a) - J_{n-1}(\beta a) H_n(\beta a) \right]$$

$$B_n = -\frac{2\psi_0 i^n}{\Delta_n} \left[n\alpha a H_{n-1}(\alpha a) J_n(\beta a) + n\beta a H_n(\alpha a) J_{n-1}(\beta a) - \alpha\beta a^2 H_{n-1}(\alpha a) J_{n-1}(\beta a) \right] \tag{34}$$

where

$$\delta_1 = -4\eta H_1(\alpha a)H_1(\beta a) + (1+\eta)\,\alpha a H_0(\alpha a)H_1(\beta a) + (1+\eta)\,\beta a H_0(\beta a)H_1(\alpha a) - \alpha\beta a^2 H_0(\alpha a)H_0(\beta a) \tag{35}$$

$$\Delta_n = n\alpha a\, H_{n-1}(\alpha a)\, H_n(\beta a) + n\beta a H_{n-1}(\beta a)H_n(\alpha a) - \alpha\beta a^2 H_{n-1}(\alpha a)H_{n-1}(\beta a) \tag{36}$$

Substitution of Equations (32) through (36) into Equations (10) and (11) yields the solution for the stresses and displacements for the rigid inclusion case.

At the boundary, where $r = a$, the dimensionless stresses τ^*_{rr}, $\tau^*_{\theta\theta}$, and $\tau^*_{r\theta}$ are simplified to

$$\tau^*_{rr} = \frac{4}{\pi}\left[- \frac{(1-\eta)H_1(\alpha a)}{\delta_1} \sin\theta + \sum_{n=2}^{\infty} \frac{i^{n+1} n\, H_n(\alpha a)}{\Delta_n} \sin n\theta \right] \tag{37}$$

$$\tau^*_{\theta\theta} = \left(1 - \frac{2}{k^2}\right) \tau^*_{rr} \tag{38}$$

$$\tau^*_{r\theta} = \frac{2}{\pi}\left\{ - \frac{i\beta^2 a^2}{\beta^3 a^3 H_1(\beta a) + 8\eta\left(\frac{\beta^2 a^2}{2} H_0(\beta a) - \beta a H_1(\beta a)\right)}\right.$$

$$- \frac{2}{\delta_1}\left[(1+\eta)H_1(\alpha a) - \alpha a H_0(\alpha a)\right]\cos\theta$$

$$\left. -2\sum_{n=2}^{\infty} \frac{i^{n+1}(-nH_n(\alpha a) + \alpha a H_{n-1}(\alpha a))}{\Delta_n}\cos n\theta\right\} \qquad (39)$$

It is to be noted that the Poisson's ratio range for common materials is $0 < \sigma < \frac{1}{2}$; therefore, $\tau^*_{\theta\theta}$ is always less than τ^*_{rr}. The dimensionless rigid body translation and rotation of the inclusion are given

$$U^*_y = \frac{i\,8\,\eta}{\beta a \delta_1 \pi}\left[H_1(\alpha a) - \frac{\alpha a}{2} H_0(\alpha a)\right] \qquad (40)$$

$$\Theta^* = - \frac{16i\eta}{\pi\beta a\left[\beta^2 a^2 H_1(\beta a) + 8\eta\left(\frac{\beta a}{2} H_0(\beta a) - H_1(\beta a)\right)\right]} \qquad (41)$$

The rotation is non-dimensionalized with respect to the dimensional coefficient of the rotation associated with the incident wave, i.e.,

$$\Omega_0 = - \frac{\beta^2 \Psi_0}{2}$$

LONG WAVELENGTH LIMIT

If the wavelength of the incident shear wave approaches infinity ($\beta \to 0$), the solutions obtained for the cavity and the rigid inclusion should reduce to the Kirsch's and Goodier's static solutions. Under pure shear τ_0, the static solution for the cavity case at the boundary is

$$\frac{\tau_{\theta\theta}}{\tau_0} = \tau^*_{\theta\theta} = -4 \sin 2\theta \tag{42}$$

and the static solution for the rigid inclusion is

$$\frac{\tau_{rr}}{\tau_0} = \tau^*_{rr} = \frac{2k^2}{k^2+1} \sin 2\theta$$

$$\frac{\tau_{r\theta}}{\tau_0} = \tau^*_{r\theta} = \frac{2k^2}{k^2+1} \cos 2\theta \tag{43}$$

$$\tau^*_{\theta\theta} = \left(1 - \frac{2}{k^2}\right) \tau^*_{rr}$$

For small arguments, the Bessel functions are approximated by the leading terms of their series. Thus, as $x \to 0$,

$$H_0(x) \to 1 + i \left(\frac{2}{\pi}\right) (\ln x - 0.11593)$$

$$H_n(x) \to \left(\frac{x}{2}\right)^n / n! \quad -i(n-1)! \quad \left(\frac{2}{x}\right)^n / \pi$$

The coefficients of sinusoidal functions for $\tau^{*}_{\theta\theta}$ in the cavity case are reduced in the limit, as $\beta a \to 0$ and $\alpha a = \frac{\beta a}{k} \to 0$, to the following form for

$n = 1$

$$\frac{\frac{-\beta^2 a^2}{2} H_1(\alpha a)}{\Delta_1} \to 0 \qquad (44)$$

$n \geq 2$

$$\frac{n(n^2-1-\frac{\beta^2 a^2}{2})H_n(\alpha a)}{\Delta_n}$$

$$\to i\pi n \left(n^2-1-\frac{\beta^2 a^2}{2}\right)(n-1)! \left(\frac{\beta a}{2}\right)^{n-2} \Big/ 4[(n-1)!]^2 \left(n^2+n-\frac{\beta^2 a^2}{4}\right)$$

$$+ \frac{(n^2-1)\alpha^2 a^2}{2}[(n-2)!]^2 + 2\left(-n^3+n-\frac{\beta^2 a^2}{2}\right)(n-2)!(n-1)!\left(1+\frac{1}{k^2}\right)$$

$$\rightarrow \begin{cases} \dfrac{i\pi}{2\left(1-\dfrac{1}{k^2}\right)} & n = 2 \\ \\ 0 & n > 2 \end{cases} \qquad (45)$$

Therefore, as $\beta a \rightarrow 0$,

$$\tau^{*}_{\theta\theta} = -4 \sin 2\theta \qquad (46)$$

which is identical to Equation (42).

The coefficients for the sinusoidal function in Equations (37) and (39) for the rigid inclusion case are reduced in the limit, as $\alpha a \rightarrow 0$ and $\beta a \rightarrow 0$, to

$$\frac{-(1-\eta)H_1(\alpha a)}{\delta_1} \rightarrow \frac{i\pi(1-\eta)\beta a}{8\eta} \rightarrow 0$$

$$\frac{nH_n(\alpha a)}{\Delta_n} \rightarrow \frac{i\pi k^2 \left(\dfrac{\beta a}{2}\right)^{n-2}}{(n-2)!(1+k^2) - \dfrac{\beta^2 a^2 (n-2)!}{n(n-1)}}$$

$$\rightarrow \begin{cases} \dfrac{i\pi k^2}{2(1+k^2)} & n = 2 \\ 0 & n > 2 \end{cases} \tag{47}$$

$$\frac{-i\beta^2 a^2}{\beta^3 a^3 H_1(\beta a) + 8\eta \left[\frac{\beta^2 a^2}{2} H_0(\beta a) - \beta a H_1(\beta a)\right]} \rightarrow -\frac{\pi}{16\eta} \beta^2 a^2 \rightarrow 0$$

$$\frac{(1+\eta) H_1(\alpha a) - \alpha a H_0(\alpha a)}{\delta_1} \rightarrow \frac{-i\pi(1+\eta)\beta a}{8\eta} \rightarrow 0 \tag{48}$$

$$\frac{-n H_n(\alpha a) + \alpha a H_{n-1}(\alpha a)}{\Delta_n} \rightarrow \frac{-i\pi k^2 \left(\frac{\beta a}{2}\right)^{n-2}}{(n-2)!\,2(1+k^2)}$$

$$\rightarrow \begin{cases} \dfrac{-i\pi k^2}{2(1+k^2)} & n = 2 \\ 0 & n > 2 \end{cases}$$

Therefore,

$$\tau^*_{\theta\theta} = \frac{2k^2}{k^2+1} \sin 2\theta$$

$$\tau^{*}_{r\theta} = \frac{2k^2}{k^2+1} \cos 2\theta$$

which are identical to Equation (43).

For the case where $\eta = 0$, a singularity will occur in the $n = 1$ term as $\beta a \to 0$. The coefficients in this case are of the form

$$\frac{H_1(\alpha a)}{\Delta_1} \sim \frac{k^2}{(1+k^2)\beta a}$$

$$\frac{-H_1(\alpha a) - \alpha a\, H_1(\alpha a)}{\Delta_1} \sim \frac{-k^2}{(1+k^2)\beta a} \qquad (49)$$

Hence, it is apparent that the stresses will become infinitely large as the wave number approaches zero for the "fixed in space" rigid inclusion.

NUMERICAL RESULTS AND DISCUSSIONS

For wavelengths other than very long or very short, the stresses and displacements are determined by the series given in Equations (18) through (20) for the cavity case and in Equations (37) through (41) for the rigid inclusion case. Numerical evaluations were carried out

on a 7090 IBM computer where the series were terminated when accuracy of 10^{-4} was achieved.

The expressions for the stresses and displacements are all of the form

$$(R + iI)\ e^{-i\omega t} = (R^2 + I^2)^{\frac{1}{2}}\ e^{-i(\omega t-\gamma)}$$

In one complete cycle, the real parts R yield the stresses at $t = 0$, and the imaginary parts I yield the stresses at $t = \frac{T}{4}$, where T is the period of the incident wave. The absolute values $(R^2 + I^2)^{\frac{1}{2}}$ are the maximum stresses which occur at an instant between $t = 0$ and $t = \frac{T}{4}$ depending on the phase angle $\gamma = \tan^{-1}\left(\frac{I}{R}\right)$.

Cavity

In this case, the only nonvanishing stress at the boundary is $\tau^*_{\theta\theta}$, therefore, it is also the maximum principle stress. Numerical results of stresses and displacements were obtained for the values of $\sigma = 0.15$, 0.25, 0.35 and dimensionless wave numbers in the range $0.1 \leq \beta a \leq 3.0$.

Fig. 2 illustrates the angular distribution of $|\tau^*_{\theta\theta}|$ for three wave numbers, $\beta a = 0.1$, 1.0 and 1.5. It is to be noted that at $\beta a = 0.1$, the stress distribution is almost identical to that of the static case, while at higher wave numbers the stress distribution is considerably distorted from the static case. Figs. 3 and 4 show how stresses at two points on the cavity $(\theta = \frac{\pi}{4}, \frac{3\pi}{4})$ vary with frequency

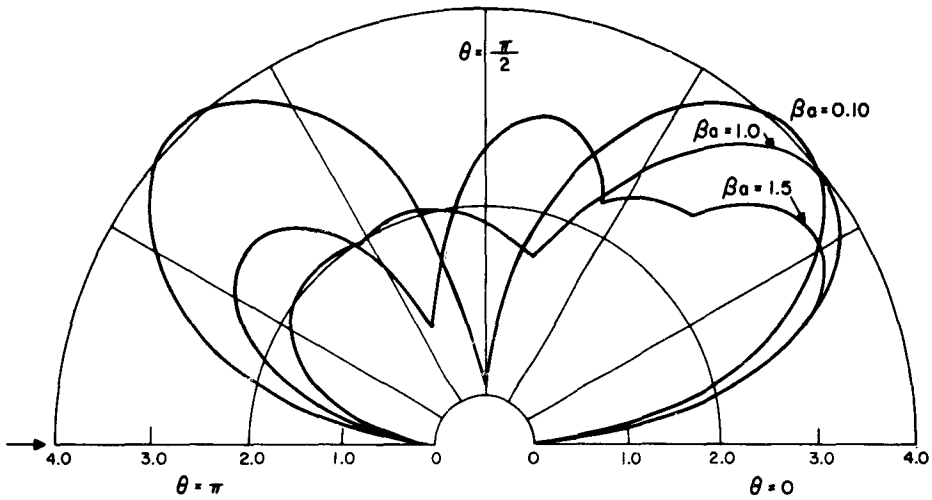

Fig. 2 Distribution of $\left|\tau^{*}_{\theta\theta}\right|$ for Various βa with $\sigma = 0.25$ (Cavity)

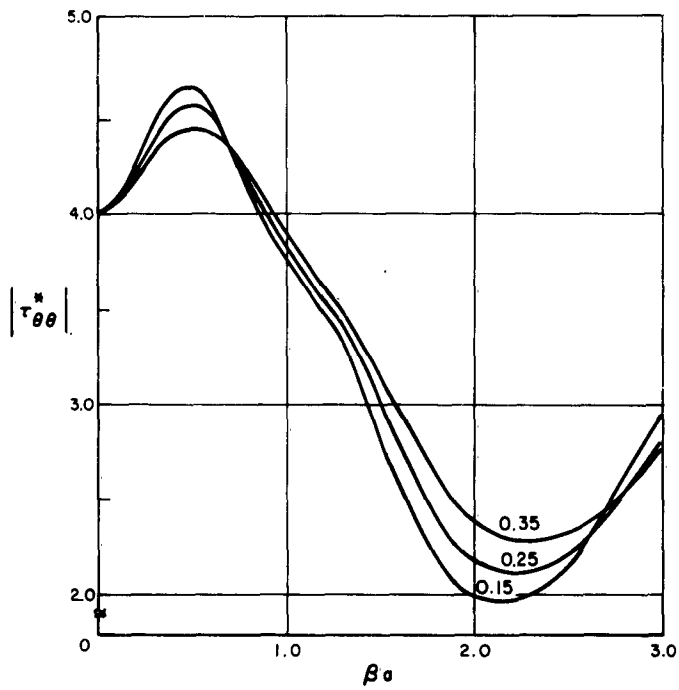

Fig. 3 $\left|\tau^{*}_{\theta\theta}\right|$ vs βa for Various σ at $\theta = \frac{\pi}{4}$ (Cavity)

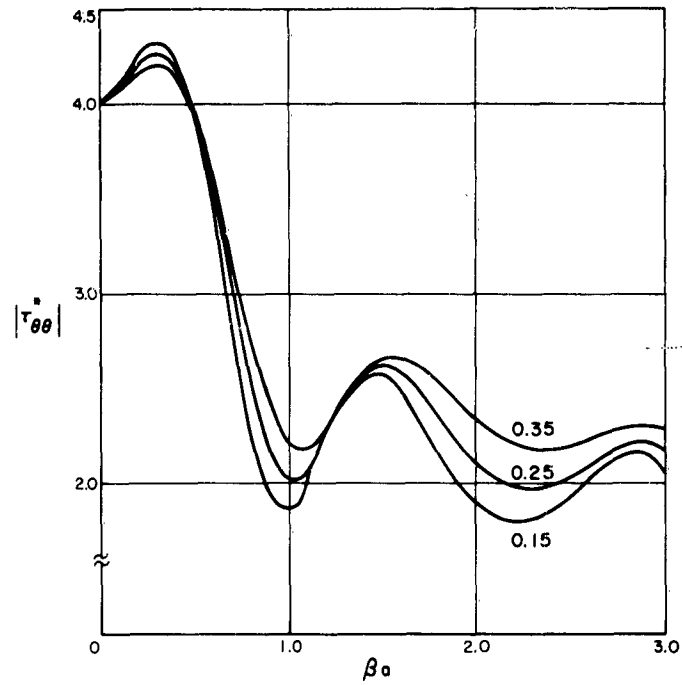

Fig. 4 $|\tau^*_{\theta\theta}|$ vs βa for Various σ at $\theta = \frac{3\pi}{4}$ (Cavity)

and the Poisson's ratio of the medium. In this case, as well as results shown in References 2, 3 and 4, the maximum dynamic stress is only 10 to 20 per cent higher than the static values, and the wave number at which the maximum occurs lies between 0.20 and 0.50.

The angular distributions of $|u_r^*|$ and $|u_\theta^*|$ for values of $\beta a = 0.10$, 1.0, and 1.5 are shown in Figs. 5 and 6. At $\beta a = 0.10$ the displacements are again the same as the static case; while at high frequency there appear to be two stationary values for $|u_r^*|$ in the

interval of $0 \leq \theta \leq \pi$, and three stationary values for $|u_\theta^*|$. Both maxima for $|u_r^*|$ and $|u_\theta^*|$ tend to shift toward the incident side as the wave number increases.

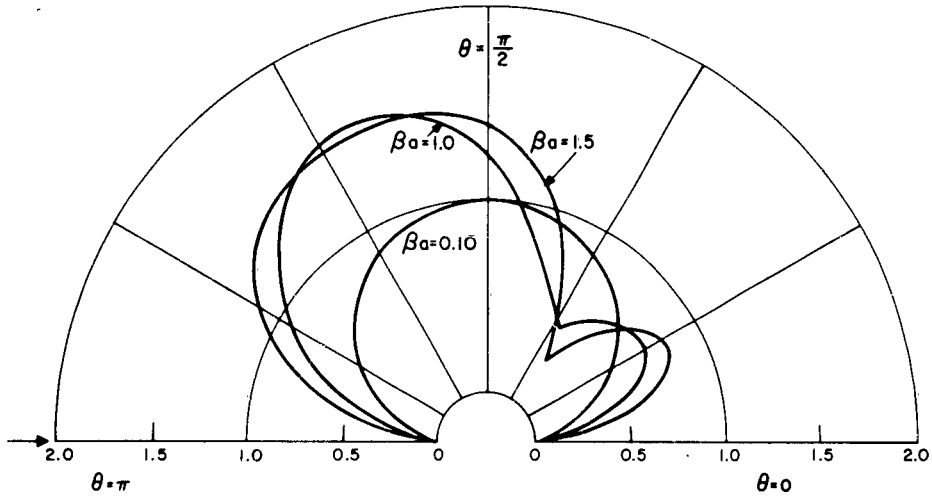

Fig. 5 Distribution of $|u_r^*|$ for Various βa with $\sigma = 0.25$ (Cavity)

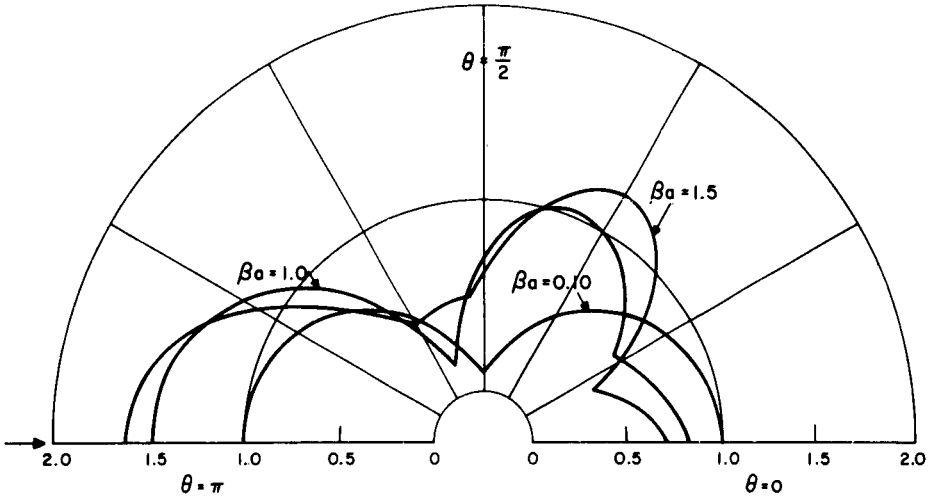

Fig. 6 Distribution of $|u_\theta^*|$ for Various βa with $\sigma = 0.25$ (Cavity)

Rigid Inclusion

Figs. 7 and 8 illustrate the angular distributions of $|\tau^*_{rr}|$ and $|\tau^*_{r\theta}|$ for two wave numbers ($\beta a = 0.1, 1.5$) and $\eta = 0.5$. At $\beta a = 0.1$ (low frequency), the distribution is nearly symmetric with respect to the x and y axes, as should be expected. At high wave numbers this symmetry does not exist, and the maximum tends to shift to the incident side of the inclusion.

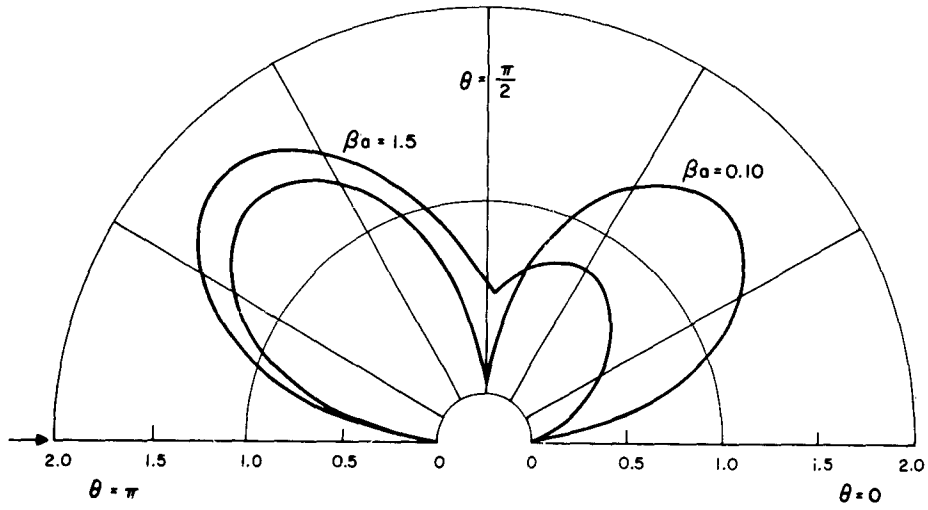

Fig. 7 Distribution of $|\tau^*_{rr}|$ for Various βa with $\sigma = 0.25$ and $\eta = 0.5$ (Rigid Inclusion)

Figs. 9 through 12 show the variation of $|\tau^*_{rr}|$, $|\tau^*_{r\theta}|$, $|\Theta^*|$, and $|U^*_y|$ as a function of wave number for various values of η. It is apparent that the density ratio η $(\frac{\rho_o}{\rho_1})$ has a large influence on

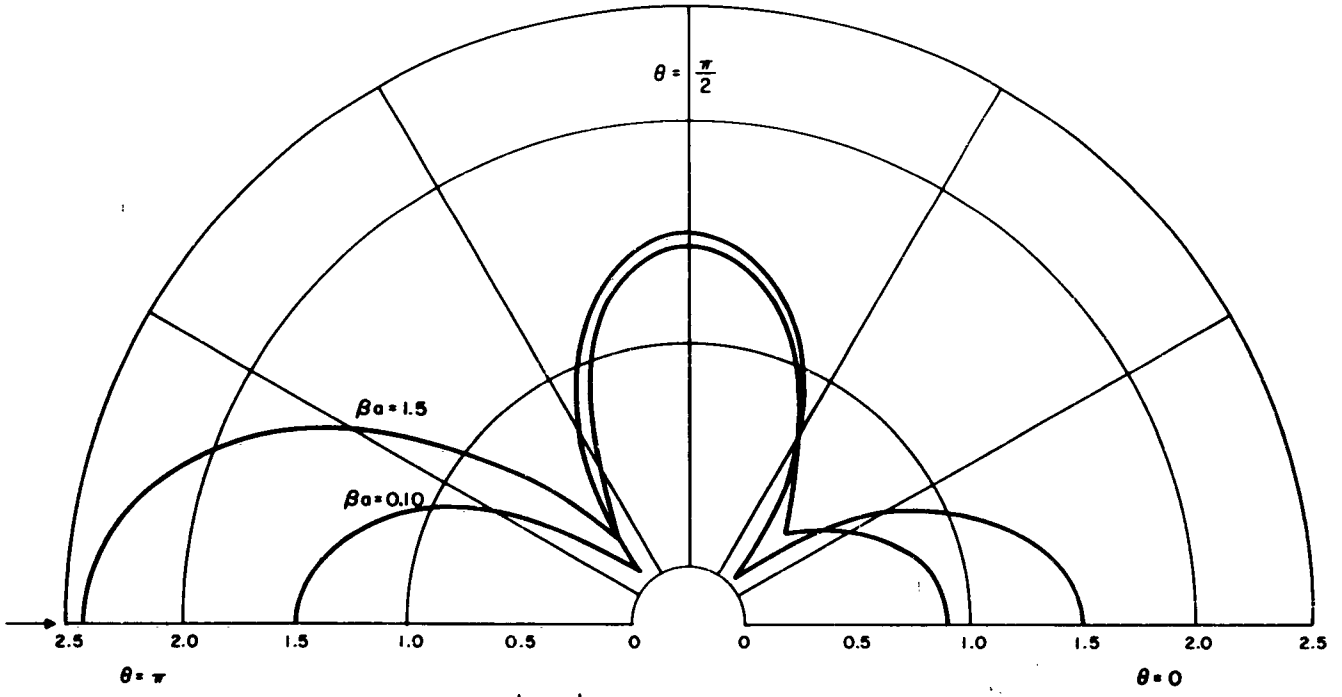

Fig. 8 Distribution of $|\tau^*_{r\theta}|$ for Various βa with $\sigma = 0.25$ and $\eta = 0.5$ (Rigid Inclusion)

the stresses, displacements, and rotation. As the density of the inclusion increases the maximum value of the stress, displacement, and rotation also increases. This increase becomes appreciably greater for density ratios below 0.5. In the case of $\eta = 0.25$, for example, the maximum dynamic stress for $|\tau^*_{rr}|$ and $|\tau^*_{r\theta}|$ in Figs. 9 and 10 are, respectively, 37 and 105 per cent greater than those under the static condition.

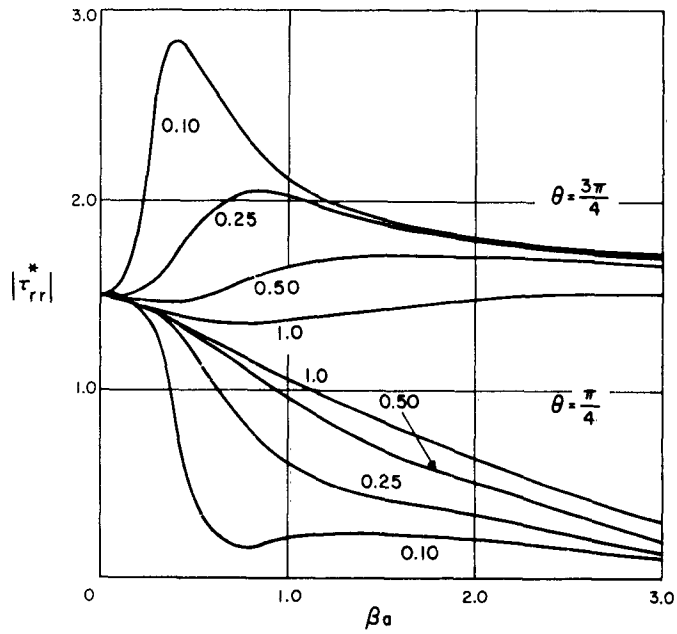

Fig. 9 $|\tau^*_{rr}|$ vs βa at $\theta = \frac{\pi}{4}, \frac{3\pi}{4}$ for Various η with $\sigma = 0.25$ (Rigid Inclusion)

It is also to be noted that there is an apparent relationship indicated between the maximum values of stresses and those of both the rigid body motions. Previous studies[3, 4, 5] have shown that there exists only one maximum for stresses as a function of frequency, which

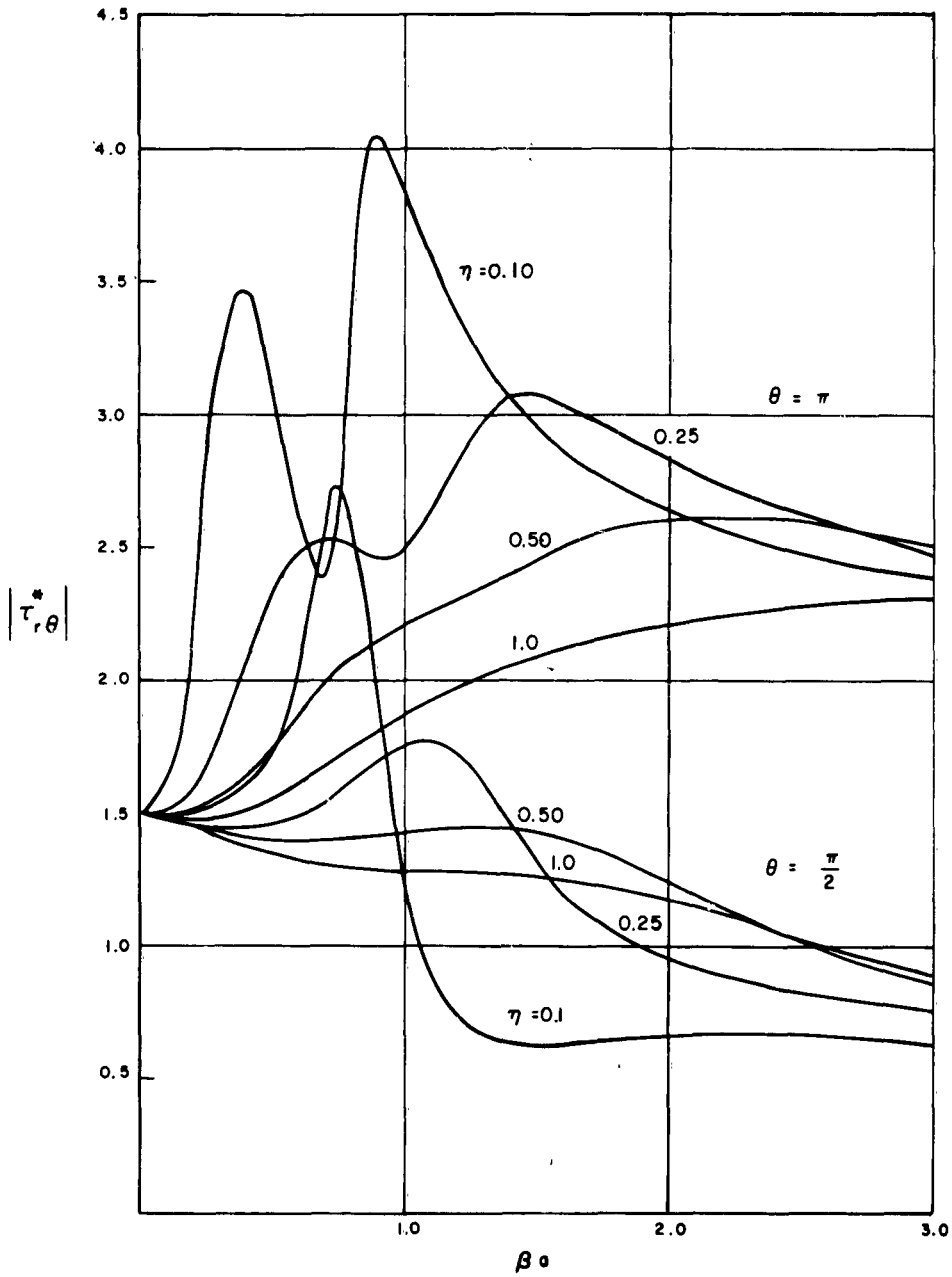

Fig. 10 $\left|\tau^*_{r\theta}\right|$ vs βa at $\theta = \pi$, $\frac{\pi}{2}$ for Various η with $\sigma = 0.25$
(Rigid Inclusion)

is also the case for $|\tau^*_{rr}|$ in Fig. 9. However, Fig. 10 shows for $|\tau^*_{r\theta}|$ at $\theta = \pi$ that there are two distinct, stationary values for $\eta = 0.10$ at two different wave numbers. By comparing these wave numbers where the peaks occur with those where the maximum of $|U^*_y|$ and $|\Theta^*|$ occur, it is apparent that the first maximum of $|\tau^*_{r\theta}|$ occurs very close to the wave number where $|U^*_y|$ is also a maximum. Furthermore, the wave number corresponding to the second maximum of $|\tau^*_{r\theta}|$ is very close to the wave number at which $|\Theta^*|$ is a maximum. These observations certainly indicate the presence of coupling between the rigid body motions and the stress at the boundary.

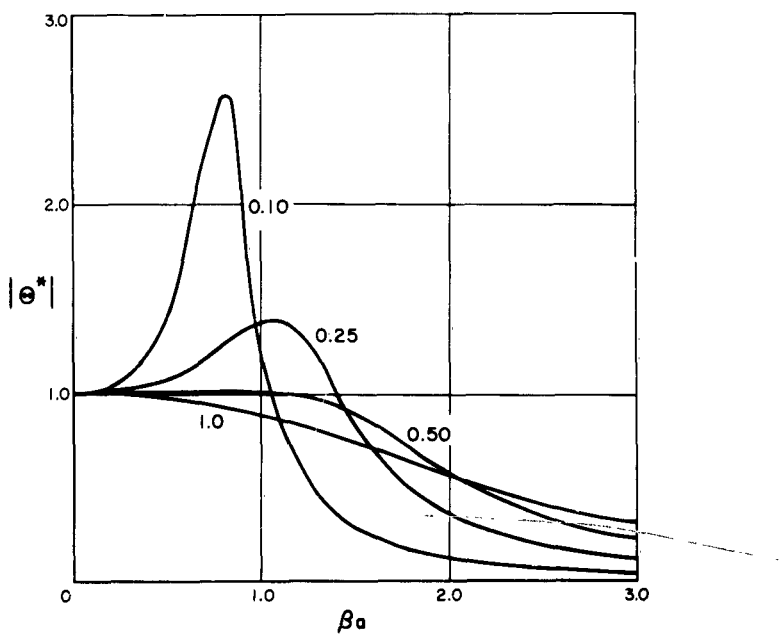

Fig. 11 $|\Theta^*|$ vs βa for Various η (Rigid Inclusion)

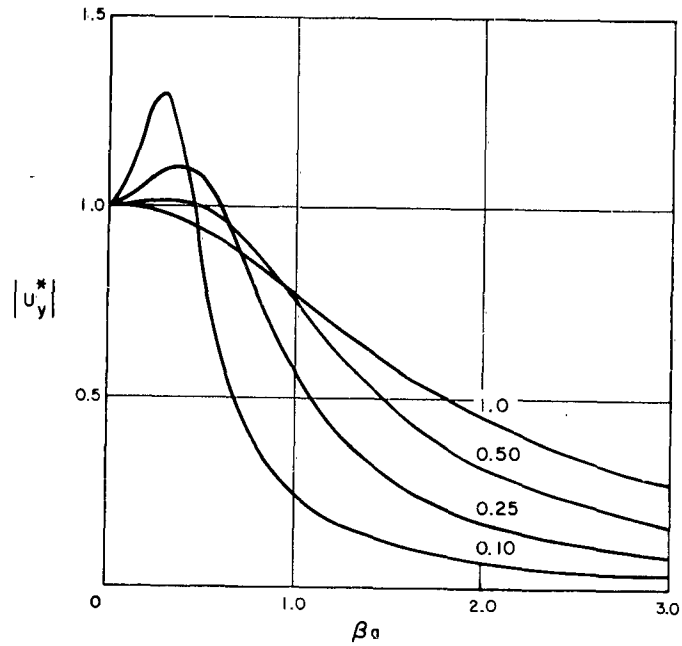

Fig. 12 $|U_y^*|$ vs βa for Various η with $\sigma = 0.25$ (Rigid Inclusion)

From Figs. 11 and 12 it is shown that the denser inclusions receive the greater rigid body motion for βa approximately less than 1.5 for $|\Theta^*|$ and 1.0 for $|U_y^*|$, but the converse is true as the wave number increases beyond these values.

REFERENCES

1. Nishmura, G. and Y. Jimbo, "A Dynamic Problem of Stress Concentration," Journal of the Faculty of Engineering, University of Tokyo, Japan, Vol. 24, 1955, p. 101.

2. Baron, M. L., H. Bleich, and P. Weidlinger, "A Theoretical Study on Ground Shock," MITRE SR-19, October 1960.

3. Pao, Yih Hsing, "Dynamic Stress Concentration in an Elastic Plate," Journal of Applied Mechanics, Vol. 29, p. 299, Series E., No. 2, June 1962.

4. Pao, Yih Hsing and C. C. Mow, "Dynamic Stress Concentration in an Elastic Plate with Rigid Circular Inclusion," Proceedings of Fourth U. S. National Congress, Berkeley, California, June 1962. MITRE SR-41, December 1961.

5. Mow, C. C. and W. L. McCabe, "Dynamic Stresses in an Elastic Cylindrical Lining of Arbitrary Thickness in an Elastic Medium," MITRE SR-57, August 1962.

6. Timoshenko, S. and J. N. Goodier, Theory of Elasticity, p. 81, Second Edition, McGraw Hill Book Co., New York, 1951.

7. Goodier, J. N., "Concentration of Stress Around Spherical and Cylindrical Inclusions and Flaws," Journal of Applied Mechanics, Vol. 1, Transaction ASME, Vol. 55, p. 39, 1933.

UNCLASSIFIED

Naval Research Laboratory. Report 5942. A VACUUM PNEUMATIC PROCESS FOR FILLING LARGE DRY CHEMICAL FIRE EXTINGUISHERS, by H.B. Peterson, R.L. Tuve, R.L. Gipe, and J.W. Porter. 13 pp. and figs., April 10, 1963.

A pneumatic conveying system has been developed for filling large fire extinguishers with dry chemical powder. The system is intended particularly for air stations and similar field establishments; it could be used for reloading extinguishers at the site of a fire. The essential components are a 1-1/2 horsepower vacuum cleaner and an especially designed device which is used in place of the extinquisher fill cap which separates the powder from the air stream, and also provides entry for a powder level gage stick.

UNCLASSIFIED (over)

1. Fire extinguishers - Maintenance

I. Peterson, H. B.
II. Tuve, R. L.
III. Gipe, R. L.
IV. Porter, J. W.

UNCLASSIFIED

Naval Research Laboratory. Report 5942. A VACUUM PNEUMATIC PROCESS FOR FILLING LARGE DRY CHEMICAL FIRE EXTINGUISHERS, by H.B. Peterson, R.L. Tuve, R.L. Gipe, and J.W. Porter. 13 pp. and figs., April 10, 1963.

A pneumatic conveying system has been developed for filling large fire extinguishers with dry chemical powder. The system is intended particularly for air stations and similar field establishments; it could be used for reloading extinguishers at the site of a fire. The essential components are a 1-1/2 horsepower vacuum cleaner and an especially designed device which is used in place of the extinquisher fill cap which separates the powder from the air stream, and also provides entry for a powder level gage stick.

UNCLASSIFIED (over)

1. Fire extinguishers - Maintenance

I. Peterson, H. B.
II. Tuve, R. L.
III. Gipe, R. L.
IV. Porter, J. W.

UNCLASSIFIED

Naval Research Laboratory. Report 5942. A VACUUM PNEUMATIC PROCESS FOR FILLING LARGE DRY CHEMICAL FIRE EXTINGUISHERS, by H.B. Peterson, R.L. Tuve, R.L. Gipe, and J.W. Porter. 13 pp. and figs., April 10, 1963.

A pneumatic conveying system has been developed for filling large fire extinguishers with dry chemical powder. The system is intended particularly for air stations and similar field establishments; it could be used for reloading extinguishers at the site of a fire. The essential components are a 1-1/2 horsepower vacuum cleaner and an especially designed device which is used in place of the extinquisher fill cap which separates the powder from the air stream, and also provides entry for a powder level gage stick.

UNCLASSIFIED (over)

1. Fire extinguishers - Maintenance

I. Peterson, H. B.
II. Tuve, R. L.
III. Gipe, R. L.
IV. Porter, J. W.

UNCLASSIFIED

Naval Research Laboratory. Report 5942. A VACUUM PNEUMATIC PROCESS FOR FILLING LARGE DRY CHEMICAL FIRE EXTINGUISHERS, by H.B. Peterson, R.L. Tuve, R.L. Gipe, and J.W. Porter. 13 pp. and figs., April 10, 1963.

A pneumatic conveying system has been developed for filling large fire extinguishers with dry chemical powder. The system is intended particularly for air stations and similar field establishments; it could be used for reloading extinguishers at the site of a fire. The essential components are a 1-1/2 horsepower vacuum cleaner and an especially designed device which is used in place of the extinquisher fill cap which separates the powder from the air stream, and also provides entry for a powder level gage stick.

UNCLASSIFIED (over)

1. Fire extinguishers - Maintenance

I. Peterson, H. B.
II. Tuve, R. L.
III. Gipe, R. L.
IV. Porter, J. W.

In trials at the Laboratory this system reduced the filling time for a 400-lb. capacity dry chemical "air-lift" extinguisher from 46 to 6 minutes, reduced dusting to a negligible amount, and allowed correct gaging of adequate charge amounts.

The simply designed separator permitted only 3.4% of the total powder weight to be carried over into the bag filter of the vacuum cleaner. This could, of course, be emptied into the shipping can used in the next charge cycle or returned to the charge during the filling process. The segregation represented by these "returnable" fines reduced the specific surface of the extinguisher charge powder only 5%, even if the fines caught by the filter bag were not returned. There is no evidence yet that this change would lower the unit efficacy of the extinguishing powder appreciably.

UNCLASSIFIED

UNCLASSIFIED

In trials at the Laboratory this system reduced the filling time for a 400-lb. capacity dry chemical "air-lift" extinguisher from 46 to 6 minutes, reduced dusting to a negligible amount, and allowed correct gaging of adequate charge amounts.

The simply designed separator permitted only 3.4% of the total powder weight to be carried over into the bag filter of the vacuum cleaner. This could, of course, be emptied into the shipping can used in the next charge cycle or returned to the charge during the filling process. The segregation represented by these "returnable" fines reduced the specific surface of the extinguisher charge powder only 5%, even if the fines caught by the filter bag were not returned. There is no evidence yet that this change would lower the unit efficacy of the extinguishing powder appreciably.

UNCLASSIFIED

UNCLASSIFIED

In trials at the Laboratory this system reduced the filling time for a 400-lb. capacity dry chemical "air-lift" extinguisher from 46 to 6 minutes, reduced dusting to a negligible amount, and allowed correct gaging of adequate charge amounts.

The simply designed separator permitted only 3.4% of the total powder weight to be carried over into the bag filter of the vacuum cleaner. This could, of course, be emptied into the shipping can used in the next charge cycle or returned to the charge during the filling process. The segregation represented by these "returnable" fines reduced the specific surface of the extinguisher charge powder only 5%, even if the fines caught by the filter bag were not returned. There is no evidence yet that this change would lower the unit efficacy of the extinguishing powder appreciably.

UNCLASSIFIED